Superconducting state in YSn_3 with a $AuCu_3$-type structure

K. Kawashima,* M. Maruyama, M. Fukuma, and J. Akimitsu
Department of Physics and Mathematics, Aoyama Gakuin University, Fuchinobe 5-10-1, Sagamihara, Kanagawa 229-8558, Japan
(Received 23 February 2010; revised manuscript received 10 June 2010; published 23 September 2010)

In this paper, the superconducting properties of YSn_3 are reported. YSn_3 has a cubic $AuCu_3$-type structure with the space group $Pm\bar{3}m$. Magnetic susceptibility, electrical resistivity, and specific-heat data showed that YSn_3 is a superconductor with a superconducting transition temperature (T_c) of 7 K. The magnetization versus magnetic field (M-H) curve shows the typical type-II superconducting behavior. The estimated lower critical field $H_{c1}(0)$ and the upper critical field $H_{c2}(0)$ are about 90 Oe and 3000 Oe, respectively. The penetration depth $\lambda(0)$ and coherence length $\xi(0)$ are calculated to be approximately 270 nm and 66 nm, respectively, using the Ginzburg-Landau equations. The estimated Sommerfeld coefficient γ_N is 7.57 mJ/mol K^2. The normalized specific heat jump $\Delta C/\gamma_N T_c$ is estimated to be about 2.19, which is higher than the value predicted by the BCS theory in the weak-coupling limit, i.e., $\Delta C/\gamma_N T_c = 1.43$. This fact indicates that superconductivity in YSn_3 exists in the strong-coupling regime. The difference between T_c of LnX_3 (X=family of 13 or 14 elements) compounds is discussed to compare their physical properties.

DOI: 10.1103/PhysRevB.82.094517 PACS number(s): 74.70.Ad, 74.25.Bt

I. INTRODUCTION

High-pressure synthesis techniques have been successfully employed in the search for new materials including superconductor in imtermetallic compounds and oxides[1–3] and enhanced T_c value for superconductor.[4] The difference in the size of the atoms in a unit cell may be the primary cause of instability of the crystal structure of some intermetallic compounds. The application of a high pressure can change the relative atomic size. Using closed system for high-pressure synthesis is effective not only for stabilizing a composition but also for expanding a solid-solution range.

$LnSn_3$ (Ln=Y and rare-earth elements) compounds are crystallized in a cubic $AuCu_3$-type structure (space group: $Pm\bar{3}m$). There are some reports on $LnSn_3$ (Ln=light rare-earth element series=La-Gd).[5–7] For example, $LaSn_3$ has been reported to exhibit superconductivity at around 6.25 K.[8] $PrSn_3$ and $NdSn_3$ have been found to order antiferromagnetically at T_N=8.6 K and 4.5 K, respectively.[9] Moreover, $PrSn_3$ has been reported to be a heavy-Fermion compound.[10] $CeSn_3$ is categorized as a dense Kondo compound with valence fluctuation.[11] In contrast, there are very few reports on the heavy rare earth series (Ln=Tb-Lu) and Y. An experiment has been conducted by Miller and Hall[12] to synthesize heavy rare-earth element tristannide compounds using a high-pressure technique, where in $LnSn_3$ (Ln=Tb, Dy, Ho, Er, and Y) compounds were successfully obtained. $YbSn_3$ single crystals have been synthesized by the Bridgman technique.[13] $YbSn_3$ shows a superconducting transition at around 3.6 K.[14] $TbSn_3$ and YSn_3 have been synthesized at P=1–7 GPa and T=400 °C–1300 °C. These two compounds also have a cubic $AuCu_3$-type structure with a lattice constant a =0.466 nm and 0.467 nm, and a density of 8.45 g/cm^3 and 7.27 g/cm^3, respectively.[15]

We focused on Ln=nonmagnetic atoms compound YSn_3. To the best of our knowledge, the physical properties of YSn_3 have not been elucidated thus far. We synthesized a polycrystalline samples of YSn_3 using a high-pressure technique and discovered that YSn_3 is a superconductor with T_c of 7 K. We performed electrical resistivity, magnetic susceptibility, and specific-heat measurements to determine the superconducting parameters of YSn_3

In this paper, we report the superconducting properties and superconducting parameters of yttrium tristannide YSn_3 prepared under a high pressure. Further, we discuss the difference between T_c of LnX_3 (X=family of 13 or 14 elements) compounds.

II. EXPERIMENTAL DETAILS

A mixture of yttrium (99.9%) and tin (99.999%) powders was encapsulated in a hexagonal boron nitride crucible (ϕ3.8 mm×8 mm). The amount of tin powder was slightly larger than that of the stoichiometric ratio of Y:Sn=1:3. Next, the encapsulated sample was subjected to high-temperature/pressure conditions using the cubic-anvil-type high-pressure equipment. In a previous study, YSn_3 has been synthesized by a melt-process method at around the peritectic temperature between Y and Sn (~500 °C).[16] The sample synthesis was performed under varying conditions of pressure (up to 5.5 GPa, the maximum pressure of the experimental apparatus) and temperature (up to 1200 °C) in order to determine the optimum condition for the sample synthesis of YSn_3. The optimum condition for the sample synthesis of YSn_3 was 700 °C–2–10 min→470 °C–10–30 min at P =5.5 GPa. After subjecting the sample to these conditions, it was quenched to room temperature before releasing the applied pressure.

The synthesized sample was analyzed by powder x-ray diffraction using a conventional x-ray spectrometer with a graphite monochromator (RINT-1000, RIGAKU). The color of the powdered sample was dark gray. Intensity data were collected with Cu $K\alpha$ radiation over a 2θ range of 10°–80° with a step width of 0.02°. Electrical resistivity measurements were performed using the conventional dc four probe method (physical property measurement system (PPMS), Quantum Design) at temperature from 2 to 300 K in an applied magnetic field of up to 10 kOe. The sample dimensions

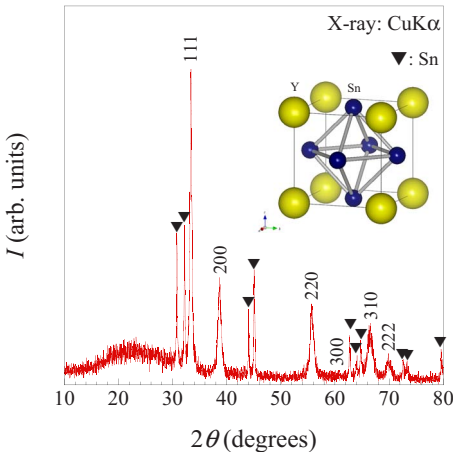

FIG. 1. (Color online) Powder x-ray diffraction pattern of synthesized YSn_3 sample. The inset shows the crystal structure of YSn_3. The solid line in the inset shows the unit cell of YSn_3. [The program VESTA was used to draw crystal structure (Ref. 18)]

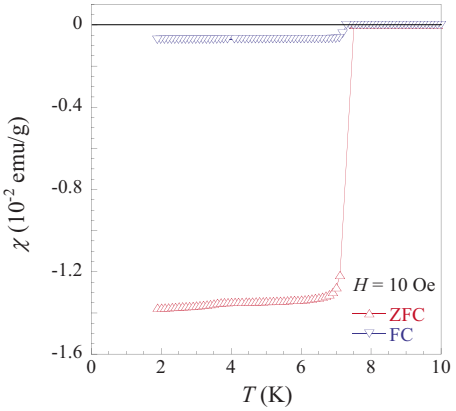

FIG. 2. (Color online) Temperature dependence of magnetic susceptibility of synthesized YSn_3 in magnetic field of 10 Oe. ZFC and FC data are measured upon warming in a field after cooling in a zero field and by cooling in a field, respectively.

for resistivity measurements were 2 mm × 1.9 mm × 1.6 mm. Electrical leads were fabricated by spot welding gold wires (ϕ25 μm) onto a polished surface of the sample. Magnetic measurements were performed by using a superconducting quantum interference device magnetometer (magnetic property measurement system (MPMS)-R2, Quantum Design) at temperatures between 2 and 15 K in an applied magnetic field of up to 3 kOe. The measurements were carried out upon warming after zero-field cooling (ZFC process) and cooling in the field (FC process). Specific-heat measurement was performed using the PPMS system (Quantum Design) in a temperature range between 0.4 and 15 K. The sample dimensions for specific-heat measurement were about 1.5 mm × 1.5 mm × 2 mm.

YSn_3 decomposes into metallic tin within 2 weeks.[12] The synthesized sample also decomposed in air. After synthesis, the sample was placed in Ar atmosphere to prevent its decomposition. The sample quality was checked one week after the synthesis. The results of powder x-ray diffraction showed that the bulk sample did not decompose and this sample exhibited a sharp superconducting transition. Consequently, the physical properties of the sample were measured within 5 days of the sample synthesis.

III. RESULTS AND DISCUSSION

Figure 1 shows the powder x-ray diffraction (PXRD) pattern of synthesized YSn_3 obtained at room temperature. The main phase is indexed as a cubic unit cell with the space group of $Pm\bar{3}m$. There are extra reflections, which belong to the impurity phase, identified as Sn. This result is consistent with that obtained in previous works.[12,17] From the intensity data from the PXRD measurement, refinement is performing to account for an admixture of Sn phase, whose weight fraction was refined to be ≈39%. The crystal structure of YSn_3 is shown in the inset of Fig. 1. The lattice parameter, a, calculated from indexes is 0.4667(4) nm. It is consistent with the data presented in a previous report.[15]

The temperature dependence of dc magnetic susceptibility under a magnetic field of 10 Oe is shown in Fig. 2. Figure 2 shows a large diamagnetic response at around 7 K, suggesting the occurrence of superconductivity, both in ZFC and FC processes. In the yttrium-tin system, intermetallic compounds having the following formulas have been identified: Y_5Sn_3 (hexagonal Mn_5Si_3-type structure), Y_5Sn_4 (orthorhombic Sm_5Ge_4-type structure), $Y_{11}Sn_{10}$ (tetragonal $Ho_{11}Ge_{10}$-type structure), YSn_2 (orthorhombic $ZrSi_2$-type structure), and YSn_3 (cubic $AuCu_3$-type structure).[16,19] The powder x-ray diffraction pattern of our sample shows that the sample includes YSn_3 as the main phase and Sn as the impurity phase. There are no additional peaks in the x-ray diffraction data. It is concluded that the large Meissner response at around 7 K originated from YSn_3 superconductor. A weak anomaly is confirmed in the ZFC data of magnetic susceptibility at around 3.8 K. This anomaly is caused by the contribution of the superconductivity of the impurity phase of Sn, whose T_c is 3.7 K.

The temperature dependence of electrical resistivity is shown in Fig. 3. The electrical resistivity data show a metallic behavior with the residual resistivity ratio (RRR): $\rho_{300\ K}/\rho_0 \sim 13$ (ρ_0 is the residual resistivity at T_c^{onset}). The onset superconducting transition temperature (T_c^{onset}) is about 7.3 K and zero resistivity is confirmed at around 7 K. The superconducting transition point is consistent with the data of magnetic susceptibility. From the results of magnetic susceptibility and electrical resistivity measurements, T_c is determined to be 7 K.

Figure 4 shows the magnetic field dependence of the magnetization of YSn_3 measured at various temperatures. The data in the inset of Fig. 4(a) shows a hysteresis, indicating that YSn_3 is a type-II superconductor. The lower critical field $H_{cl}(T)$ was determined from the magnetic field versus magnetization (M-H) curve measured at various temperatures. As shown in Fig. 4(a), $H_{c1}(T)$ was defined as a magnetic field at which the diamagnetic magnetization deviates from a linear relation with the magnetic field. Figure 4(b) shows $H_{c1}(T)$ as a function of $(T/T_c)^2$. $H_{c1}(T)$ was fitted by the relation

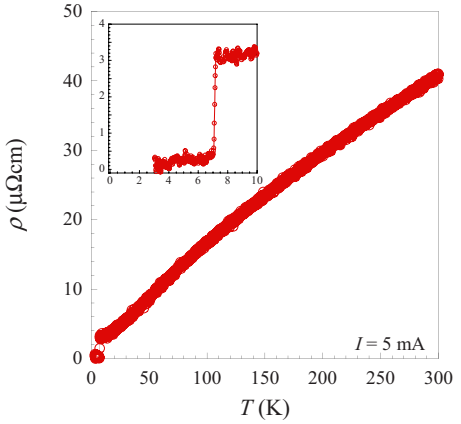

FIG. 3. (Color online) Temperature dependence of zero-field electrical resistivity (measuring current I=5 mA) of synthesized YSn_3. The inset shows an enlarged view of the plot in a low-temperature range ($T \leq 10$ K).

$$H_{c1}(T) = H_{c1}(0)[1 - (T/T_c)^2] \quad (1)$$

using the Ginzburg-Landau (GL) theory, where $H_{c1}(0)$ is H_{c1} at 0 K. $H_{c1}(0)$ was determined to be about 90 Oe. The penetration depth $\lambda(0)$ was calculated to be approximately 270 nm from the relation, $\mu_0 H_{c1} \sim \phi_0/\pi\lambda^2$, where μ_0 and ϕ_0 are the magnetic permeability of the vacuum and quantum flux, respectively.

Figure 5 shows the temperature dependence of electrical resistivity under different magnetic fields up to 3000 Oe. T_c and $H_c(0)$ values for Sn are 3.7 K and about 300 Oe, respectively. There is no influence of the impurity phase, Sn, on these resistivity data. The magnetic fields were applied above T_c, and the data were obtained upon cooling. T_c^{onset} and zero resistivity temperature (T_c^{zero}) shift to lower temperatures as the magnetic field increases. The transition widths remain almost unchanged up to high magnetic fields. T_c is determined at a 50% decrease from the normal-state resistivity value, and transition width is taken as the temperature interval between 10% and 90% of the transition.

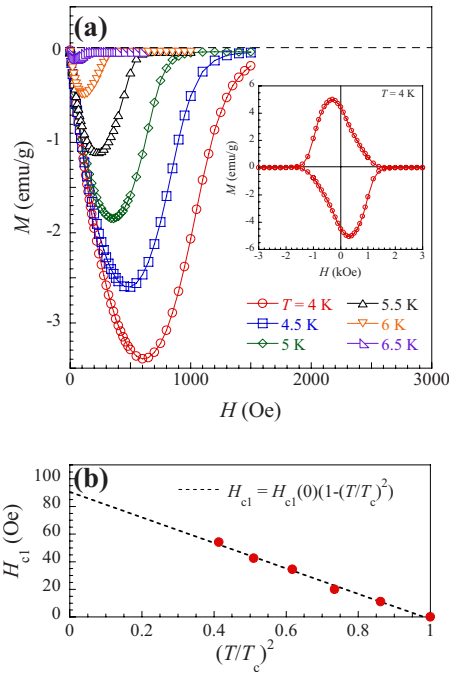

FIG. 4. (Color online) (a) Magnetic field dependence of magnetization (M-H curve) of synthesized YSn_3 at various temperatures. The inset of Fig. 4(a) shows the M-H curve at a high magnetic field. (b) Lower critical field H_{c1} as a function of $(T/T_c)^2$. The dotted line shows a linear fit to Eq. (1).

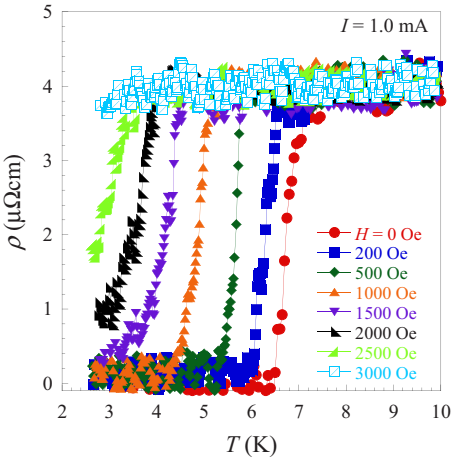

FIG. 5. (Color online) Temperature dependences of electrical resistivity (measuring current I=1 mA) of synthesized YSn_3 at various magnetic fields.

Figure 6 shows the H-T phase diagram of the superconducting state of YSn_3. The electrical resistivities are measured under various magnetic fields for two different samples. The data show a linear temperature dependence at temperatures between 3 K and near T_c. The gradient dH_{c2}/dT at around T_c is found to be about −600 Oe/K. On the basis of the relation $H_{c2} \sim -0.69 \times (dH_{c2}/dT) \times T_c$ for a type-II superconductor in the dirty limit,[20,21] the $H_{c2}(0)$ value is found to be about 3000 Oe. From these data, $\xi(0)$ value is calculated to be ~66 nm using the relation $H_{c2}(0) = \Phi_0/2\pi\xi^2$, where Φ_0 is the flux quantum. The GL parameter κ_{GL} is estimated to be 4.1 using the relation $\kappa_{GL} = \lambda/\xi$.

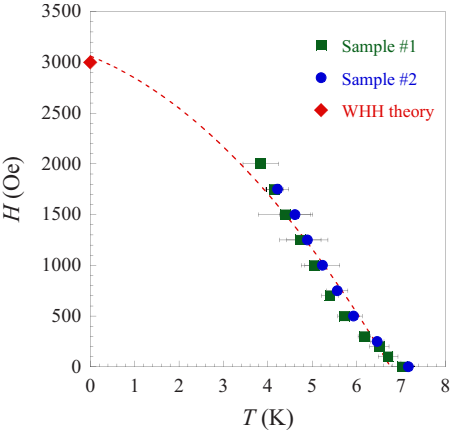

FIG. 6. (Color online) H-T phase diagram deduced from electrical resistivity of YSn_3 under various magnetic fields. The dashed curve shows a fit to the WHH theory.

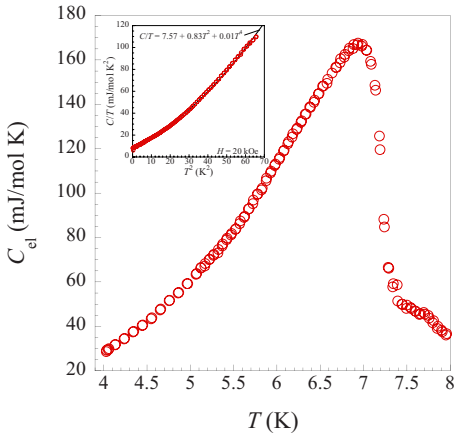

FIG. 7. (Color online) Temperature dependence of electronic specific heat of YSn_3. The inset shows the normal-state specific heat under a magnetic field H of 20 kOe as a function of temperature. The solid line shows a fit to the experimental data using the Debye formula [Eq. (2)].

Figure 7 shows the temperature dependence of the electronic specific heat C_{el} of YSn_3 at $H=0$ Oe. The inset of Fig. 7 shows the normal-state specific heat obtained by applying a magnetic field $H=20$ kOe $\gg H_{c2}$. At $H=0$ Oe, specific-heat data show the bulk superconducting feature as indicated by the clear jump of C_P at around T_c. T_c of 7 K determined from the midpoint of the specific-heat jump is consistent with the value obtained from the other measurements. At $H=20$ kOe, the specific heat jump is completely suppressed, resulting in the disappearance of superconductivity in YSn_3. A clear deviation from the Debye T^3 law is observed in the normal state C_P, which can be attributed to the contribution of the low-lying Einstein phonon modes.[22]

In order to take into account the normal state C_{ph} (lattice part), we fitted the data obtained at $H=20$ kOe by a polynomial

$$C_P/T = (C_{el} + C_{ph})/T = \gamma_N + \beta T^2 + \delta T^4 \qquad (2)$$

with the Sommerfeld coefficient of the normal-state specific heat γ_N and the coefficient of the phononic contribution β and δ as adjustable parameters. β is related to the Debye temperature $\theta_D(0)$ via $\beta=(12/5)N\pi^4R\theta_D^{-3}$, where $R=8.314$ J/mol K denotes the gas constant and $N=4$ is the number of atoms per formula unit for YSn_3. We carefully subtracted the contribution of Sn to the total sample capacity.[23] From this fit, we deduced $\gamma_N=7.57$ mJ/mol K^2, $\beta=0.83$ mJ/mol K^4, and $\delta=0.01$ mJ/mol K^6. We calculated the corresponding Debye temperature θ_D to be approximately 210 K.

In the superconducting state, the electronic specific heat C_{el} of YSn_3 can be obtained after subtracting the phononic contribution from the total specific heat: $C_{el}=C_P^{YSn_3}-C_{ph}$. C_{ph} data are obtained from the fitting result of Eq. (2). The normalized specific-heat jump $\Delta C/\gamma_N T_c$ is calculated to be about 2.19 using $\gamma_N=7.57$ mJ/mol K^2 and $T_c=7$ K. For the weak-coupling limit of the BCS theory, $\Delta C/\gamma_N T_c$ is 1.43.[24] The calculated $\Delta C/\gamma_N T_c$ value is higher than that predicted by the BCS theory in the weak-coupling limit, clearly indicating enhanced electron-phonon coupling strength.

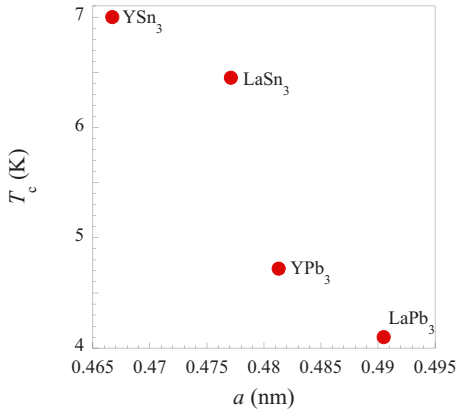

FIG. 8. (Color online) T_c of LnX_3 compounds with X=family of 14 elements of Sn^{4+} and Pb^{4+} as a function of lattice constant, a.

Here, we compare YSn_3 superconductor with other LnX_3 (Ln=La, Yb, and Y, X=family of 13 elements of In^{3+} and Tl^{3+} or family of 14 elements of Sn^{4+} and Pb^{4+}) superconductors with a $AuCu_3$-type structure to elucidate the superconducting state of LnX_3.

The compounds YIn_3, YTl_3, and YPb_3 have been found to exhibit superconductivity with T_c of 0.78 K, 1.5 K, and 4.72 K, respectively. T_c of LnX_3 compounds with X=family of 14 elements of Sn^{4+} and Pb^{4+} is higher than that of LnX_3 compounds with X=family of 13 elements of In^{3+} and Tl^{3+}.[25,26] YSn_3 has the highest T_c in the YX_3 system, similar to other LnX_3 compounds. A previous study showed that T_c depends on the concentration of valence electrons, n.[27] T_c becomes relatively high near $n=3.75$, e.g., in YPb_3, $LaSn_3$, and $LaPb_3$ ($T_c=4.1$ K), and decreases rapidly with increasing concentration of X=family of 13 element of In^{3+} or Tl^{3+} in the $Ln(In_{1-x}Sn_x)_3$, $Ln(Tl_{1-x}Pb_x)_3$, and $Ln(In_{1-x}Pb_x)_3$ systems. However, compounds with $0.5 \leq x$ ($3.5 \leq n$) in the $Y(In_{1-x}Sn_x)_3$ system could not be synthesized because high-pressure synthesis was not used. T_c of $Y(In_{1-x}Sn_x)_3$ increases slowly from 0.78 K $\sim$1.9 K with increasing Sn^{4+} concentration. The n vs T_c diagram for the $Y(In_{1-x}Sn_x)_3$ system is obtained in the present study.

The difference between T_c of the compounds of LnX_3 for X=family of 13 elements of In^{3+} and Tl^{3+} and for X=family of 14 elements of Sn^{4+} and Pb^{4+} is clearly related to the density of state from the X site ion. Although the Sommerfeld constant γ_N of $LnPb_3$ compounds is larger than that of $LnSn_3$, T_c of $LnPb_3$ compounds is lower than that of $LnSn_3$ compounds in LnX_3 (X=family of 14 elements) compounds with $n=3.75$. Consequently, phononic contribution such as the Debye frequency and electron-phonon coupling strength to the superconducting state are mainly responsible for the difference in T_c of LnX_3 compounds for X=family of 14 elements. Figure 8 shows T_c of LnX_3 for X=family of 14 elements of Sn^{4+} and Pb^{4+} compounds as a function of each lattice constant a. The lattice constant a of the compounds of LnX_3 for X=family of 14 elements with $n=3.75$, YSn_3, YPb_3, $LaSn_3$, and $LaPb_3$ ($T_c=4.1$ K) is 0.467 nm, 0.481 nm, 0.477 nm, and 0.491 nm, respectively. YSn_3 has the highest T_c among the compounds of LnX_3 for X=family of

14 elements. T_c increases with the decreasing lattice constant. The phononic contribution to the superconducting state is enhanced with the decreasing lattice constant and atomic distance for *Ln-Ln*, *Ln-X*, and *X-X*.

IV. CONCLUSIONS

In this paper, the superconducting properties of YSn_3 with a $AuCu_3$-type structure are reported. The data for the superconducting state are obtained from electrical resistivity, dc magnetic susceptibility, and specific-heat measurements. A superconducting transition is confirmed at around 7 K and a specific-heat anomaly is clearly observed at T_c indicating the bulk nature of superconductivity. The *M-H* curve at 4 K for YSn_3 shows the typical type-II superconducting behavior. The estimated $H_{c1}(0)$ value is about 90 Oe. The penetration depth λ is calculated to be approximately 270 nm. The *H-T* phase diagram is also obtained. The upper critical field $H_{c2}(0)$ is estimated to be ~3000 Oe using the Werthamer-Helfand-Hohenberg (WHH) prediction. The coherence length is calculated to be about ξ=66 nm. The normalized specific-heat jump $\Delta C/\gamma T_c$ is estimated to be about 2.19, which is higher than 1.43, the value predicted by the BCS theory. The determined superconducting parameters are listed in Table I. The electron-phonon coupling strength for superconductivity in YSn_3 is in the strong-coupling regime. T_c systematically changes with the decreasing lattice constant of the superconductor of LnX_3 with X=family of 14 elements. It is concluded that the difference between T_c of LnX_3 compounds can be attributed to the difference in the phononic contribution to the superconducting state.

TABLE I. Normal and superconducting parameters of YSn_3.

T_c	7 K
$H_{c1}(0)$	90 Oe
$H_{c2}(0)$	3000 Oe
λ	270 nm
ξ	66 nm
κ_{GL}	4.1
$\Delta C/\gamma_N T_c$	2.19
γ_N	7.57 mJ/mol K^2
β	0.83 mJ/mol K^4
θ_D	210 K

ACKNOWLEDGMENTS

This work was partially supported by a Grant-in-Aid for Scientific Research, a Grant-in-Aid for Specially Promoted Research, and the Private University High-Tech Reseach Center Program funded by the Ministry of Education, Culture, Sports, Science and Technology, Japan.

*kawaken@phys.aoyama.ac.jp

[1] S. Yamanaka, E. Enishi, H. Fukuoka, and M. Yasukawa, Inorg. Chem. **39**, 56 (2000).
[2] H. Fukuoka and S. Yamanaka, Phys. Rev. B **67**, 094501 (2003).
[3] Z. Hiroi, N. Kobayashi, and M. Takano, Nature (London) **371**, 139 (1994).
[4] G. Amano, S. Akutagawa, T. Muranaka, Y. Zenitani, and J. Akimitsu, J. Phys. Soc. Jpn. **73**, 530 (2004).
[5] A. Rossi, Atti Accad. Naz. Lincei, Cl. Sci. Fis., Mat. Nat., Rend. **17**, 839 (1933).
[6] E. Zintl and S. Neumayr, Z. Elektrochem. Angew. Phys. Chem. **39**, 86 (1933).
[7] I. R. Harris and G. V. Raynor, J. Less-Common Met. **9**, 7 (1965).
[8] R. J. Gambino, N. R. Stemple, and A. M. Toxen, J. Phys. Chem. Solids **29**, 295 (1968).
[9] G. K. Shenoy, B. D. Dunlap, G. M. Kalvius, A. M. Toxen, and R. J. Gambino, J. Appl. Phys. **41**, 1317 (1970).
[10] R. Settai, K. Sugiyama, A. Yamaguchi, S. Araki, K. Miyake, T. Takeuchi, K. Kindo, Y. Onuki, and Z. Kletowski, J. Phys. Soc. Jpn. **69**, 3983 (2000).
[11] A. P. Murani, Phys. Rev. B **28**, 2308 (1983).
[12] K. Miller and H. T. Hall, Inorg. Chem. **11**, 1188 (1972).
[13] J. C. P. Klaasse, R. T. Meijer, and F. R. de Boer, Solid State Commun. **33**, 1001 (1980).
[14] I. Sakamoto, S. Ohara, I. Oguro, and S. Maruno, Physica B **230-232**, 286 (1997).
[15] E. Y. Tonkov, *High Pressure Phase Transformations: A Handbook* (Gordon and Breach Science Publications, PA, 1992), Vol. 2.
[16] F. A. Schmidt and D. McMasters, J. Less-Common Met. **15**, 1 (1968).
[17] F. Borsa, R. G. Barnes, and R. A. Reese, Phys. Status Solidi **19**, 359 (1967).
[18] K. Momma and F. Izumi, J. Appl. Crystallogr. **41**, 653 (2008).
[19] D. Niculescu, I. Bradea, O. Ivanciu, and E. Cruceanu, J. Less-Common Met. **42**, 311 (1975).
[20] N. R. Werthamer, E. Helfand, and P. C. Hohenberg, Phys. Rev. **147**, 295 (1966).
[21] K. Maki, Phys. Rev. **148**, 362 (1966).
[22] J. S. Kim, R. K. Kremer, L. Boeri, and F. S. Razavi, Phys. Rev. Lett. **96**, 217002 (2006).
[23] The specific-heat measurements were carried out on a piece of a sample, which was also characterized by powder x-ray diffraction. The sample contained two phases: YSn_3 (the majority phase) and Sn (the impurity phase). The contribution of the sample to the measured specific heat C_P can be determined using C_P $(\mu J/Kg^{-1})=xC_P^{YSn_3}+(1-x)C_P^{Sn}$, where x and $1-x$ are the weight fractions of YSn_3 and Sn, respectively. x was determined from the ratio of intensity of powder x-ray diffraction patterns of YSn_3 and Sn. C_P^{Sn} was determined independently from previous reports (C. A. Bryant and P. H. Keesom, Phys. Rev. **123**, 491 (1961).
[24] M. Tinkham, *Introduction to Superconductivity*, 2nd ed. (McGraw-Hill, New York, 1996).
[25] E. Bucher, K. Andres, J. P. Maita, and G. W. Hull, Jr., Helv. Phys. Acta **41**, 723 (1968).
[26] E. E. Havinga, Phys. Lett. A **28**, 350 (1968).
[27] E. E. Havinga, H. Damsma, and M. H. Van Maaren, J. Phys. Chem. Solids **31**, 2653 (1970).